


RESEARCH

Open Access



Identify truly high-risk TP53-mutated diffuse large B cell lymphoma patients and explore the underlying biological mechanisms

Kai-Xin Du^{1,2,3†}, Yi-Fan Wu^{1,2,3†}, Wei Hua^{1,2,3}, Zi-Wen Duan^{1,2,3}, Rui Gao^{4,5}, Jun-Heng Liang⁶, Yue Li^{1,2,3}, Hua Yin^{1,2,3}, Jia-Zhu Wu^{1,2,3}, Hao-Rui Shen^{1,2,3}, Li Wang^{1,2,3}, Yang Shao⁶, Jian-Yong Li^{1,2,3}, Jin-Hua Liang^{1,2,3*} and Wei Xu^{1,2,3*} 

Abstract

TP53 mutation (*TP53*-mut) correlates with inferior survival in many cancers, whereas its prognostic role in diffuse large B-cell lymphoma (DLBCL) is still in controversy. Therefore, more precise risk stratification needs to be further explored for *TP53*-mut DLBCL patients. A set of 2637 DLBCL cases from multiple cohorts, was enrolled in our analysis. Among the 2637 DLBCL patients, 14.0% patients (370/2637) had *TP53*-mut. Since missense mutations account for the vast majority of *TP53*-mut DLBCL patients, and most non-missense mutations affect the function of the P53 protein, leading to worse survival rates, we distinguished patients with missense mutations. A *TP53* missense mutation risk model was constructed based on a 150-combination machine learning computational framework, demonstrating excellent performance in predicting prognosis. Further analysis revealed that patients with high-risk missense mutations are significantly associated with early progression and exhibit dysregulation of multiple immune and metabolic pathways at the transcriptional level. Additionally, the high-risk group showed an absolutely suppressed immune microenvironment. To stratify the entire cohort of *TP53*-mut DLBCL, we combined clinical characteristics and ultimately constructed the *TP53* Prognostic Index (TP53PI) model. In summary, we identified the truly high-risk *TP53*-mut DLBCL patients and explained this difference at the mutation and transcriptional levels.

Keywords Diffuse large B cell lymphoma, *TP53*, Missense mutation, Prognostic index, Biological mechanism

[†]Kai-Xin Du and Yi-Fan Wu contributed equally to this work.

*Correspondence:

Jin-Hua Liang

liangjinhua1990@126.com

Wei Xu

xuwei10000@hotmail.com

¹Department of Hematology, The First Affiliated Hospital of Nanjing Medical University, Jiangsu Province Hospital, Nanjing 210029, China

²Key Laboratory of Hematology, Nanjing Medical University, Nanjing 210029, China

³Collaborative Innovation Center for Cancer Personalized Medicine, Nanjing 210029, China

⁴Department of Endocrinology, The First Affiliated Hospital of Nanjing Medical University, Jiangsu Province Hospital, Nanjing 210029, China

⁵Oxford Centre for Diabetes, Endocrinology and Metabolism, University of Oxford, Churchill Hospital, Oxford OX3 7LE, UK

⁶Nanjing Geneseeq Technology Inc, Nanjing, Jiangsu, China



Introduction

Diffuse large B-cell lymphoma (DLBCL) is the most common lymphoid malignancy and characterized by pronounced genetic and clinical heterogeneity [1]. According to the cell-of-origin (COO) classification based on gene expression profiling, this disease can be classified into activated B-cell-like (ABC), germinal center B-cell-like (GCB), and unclassified (UNC) subtypes [2]. However, the COO classification has not been satisfied for clinical prognosis and targeted therapy in clinically [3–7]. With the development of next-generation gene sequencing (NGS) technology, Staudt et al. had developed Lymph-Gen genetic subtype classifier for DLBCL [8]. DLBCL can be divided into seven gene-subtypes with different prognosis and corresponding potential targeted therapy drugs.

TP53 mutations correlate with inferior survivals in many cancers including lymphomas [9–14]. *TP53* is the most frequently mutated gene in DLBCL enriched in A53 subtype and also could be found in other gene subtypes [8, 15]. However, A53 subtype which has fatal prognostic cannot be identified using NGS technology which was used mostly in clinical practice. Therefore, detailed prognosis should be determined for *TP53* mutations in DLBCL in order to provide a more accurate prognosis. Hong Y et al. found that *TP53* mutations correlate with inferior overall survival (OS) and progression-free survival (PFS) in DLBCL patients [11]. Despite the fact that they showed a statistically significant difference between the two groups, it can be seen that the two curves are substantially close to one another. It has also been our experience in clinical practice that not all patients with *TP53* mutations have a poor prognosis. All these phenomenon leads us to speculate that whether more precise risk stratification for *TP53* mutant (*TP53*-mut) DLBCL patients can be investigated using clinical and genetic characteristics. In the present study, we aim to develop the prognostic index (PI) to identify truly high-risk *TP53*-mut DLBCL patients and elucidate the potential underlying mechanisms of different prognosis.

Methods and materials

Study group

Public database resources

The available clinical information and corresponding mutation data of B cell lymphoma patients were retrieved and obtained from published articles. Non-DLBCL patients were excluded. Ultimately, 2637 DLBCL patients in six cohorts were enrolled in the final analysis, including Lacy S et al. cohort [15, 16] ($N=839$), Reddy A et al. cohort [17] ($N=1001$), Dubois S et al. cohort [18] ($N=361$), Pedrosa L et al. cohort [19] ($N=84$), Chapuy B et al. cohort [1] ($N=304$) and The Cancer Genome Atlas (TCGA, <https://portal.gdc.cancer.gov/>) cohort ($N=48$)

(Fig. 1). Cancer cell lines containing 21 DLBCL cell lines mutation and RNA sequencing (RNA-seq) data (Cancer Cell Line Encyclopedia, CCLE) were downloaded from the Broad Institute DepMap Portal (<https://depmap.org/portal/>).

JSPH cohort

Our study cohort consists of 108 patients with DLBCL according to the World Health Organization classification criteria between 2022 and 2023 in the First Affiliated Hospital of Nanjing Medical University (Jiangsu Province Hospital, JSPH). Among the 108 DLBCL patients, all tumor tissue samples were collected to perform NGS, while a total of 103 DLBCL samples were analyzed the gene expression levels using RNA-seq.

To obtain additional information regarding the mutations and functions of *TP53*, we retrieved the *TP53* database (<https://TP53.isbcgc.org/>, originally IARC database) for mutation site information. For the analysis, we selected 13 mutation-related factors, including exon, multi-locus mutation, with copy number variation (CNV), splice site mutation, Cytosine-phosphate-Guanine (CpG) site mutation, nucleotide change, transition/transversion, hotspot mutation, structural motif, trans-activation class, dominant-negative effect (DNE)_ loss-of-function (LOF) class, structure function class, and variant allele frequency (VAF). Pay particular attention to the following detail, which the hotspot mutations are pan-cancer hotspot mutations identified by Chang et al. [20], and are not DLBCL-specific hotspot mutations.

Patient characteristics

In enrolled patients from the 6 public databases, it was possible to retrieve all or part of the clinical data. The clinical characteristics, including age, gender, Ann Arbor stage, Eastern Cooperative Oncology Group (ECOG), No. of extranodal involvement, serum lactate dehydrogenase (LDH) level, International Prognostic Index (IPI), cell of origin (COO) subtype, LymphGen genetic subtype, treatment response and PFS or OS.

Construction of model by integrative machine learning approaches

The whole dataset was randomly divided into a training set and a testing set in a 4:1 ratio, ensuring a balanced distribution of clinical characteristics between the two groups. A total of ten machine learning algorithms were employed, including Lasso, Ridge, stepwise Cox, CoxBoost, random survival forest (RSF), elastic net (Enet), partial least squares regression for Cox (plsRcox), supervised principal components (SuperPC), generalized boosted regression modeling (GBM), and survival support vector machine (survival-SVM). On the basis of a tenfold cross-validation framework, we arranged 150

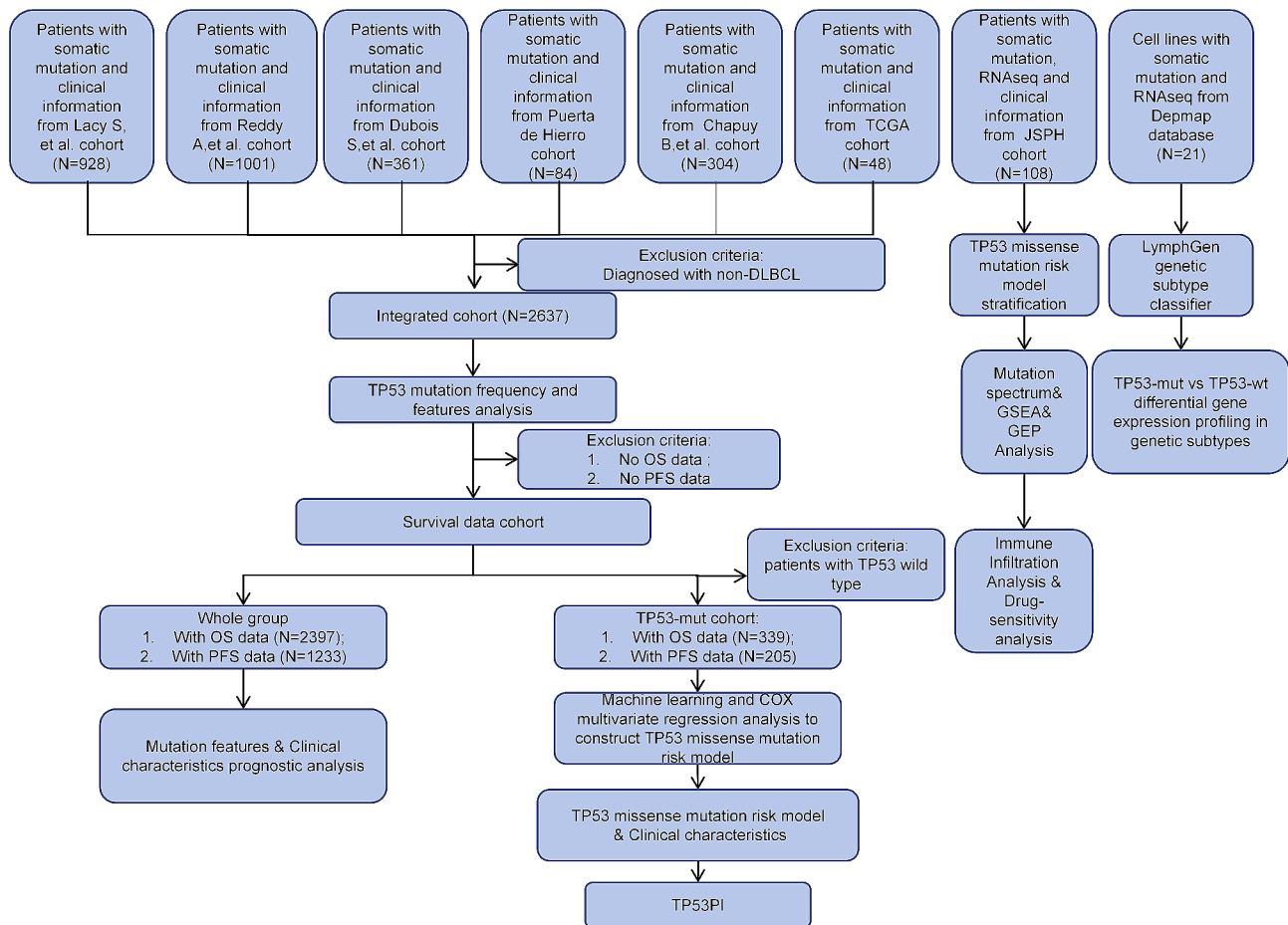


Fig. 1 Flow chart of data analysis. TCGA, The Cancer Genome Atlas; DLBCL, diffuse large B-cell lymphoma; OS, overall survival; PFS, progression free survival; *TP53*-mut, mutated *TP53*; *TP53*PI, *TP53* prognostic index; GSEA, Gene Set Enrichment Analysis; GEP, Gene Expression Profile; *TP53*-wt, wild-type *TP53*

combinations of these 10 algorithms in the training dataset for the purpose of variable selection and the construction of models. For each model, we calculated its C index both the training and the testing sets. We then ranked the models according to their predictive performance based on the mean C index. We selected a combination of algorithms with both robust performance and clinically translational significance. We assessed the models precision discrimination and accuracy using receiver operator characteristic curve (ROC) curves, the C index, and calibration curves.

Mutation analysis

Mutation analysis was performed with genomic DNA extracted from tumor tissue samples in all DLBCL patients of JSPH cohort using clinically validated NGS mutation panels.

Library construction

Libraries were constructed by using the KAPA Hyper DNA Library Prep Kit (KAPA Biosystem, KK8504) and dual-indexed sequencing libraries were generated and

cleaned by polymerase chain reaction (PCR) amplifications with KAPA HiFi Hot start-ready Mix (KAPA, KK2602) and purification Beads (Corning, AxyPrep Fragment Select-I kit, 14223162), respectively.

NGS

As the capture probes, our panels covered 475 leukemia- and lymphoma-related genes (Table S1). 1 μ g of each fragment was mixed with 5 μ g of salmon sperm DNA, 5 μ g of human Cot-1 DNA and 1 unit adaptor-specific blocker DNA in hybridization buffer and heated for 10 min at 95°C and held for 5 min at 65°C in the thermocycler. Following adding capture probes, the mixture was rest for 5 min and then heated to 65°C for 16–18 h. The captured targets were separated by pulling down the biotinylated probe/target hybrids using streptavidin-coated magnetic beads, and the off-target library was removed by a washing buffer after hybridization. We amplified the captured library from the washed beads for 6–8 cycles, purified the products by AMPure XP beads and sized them on bioanalyzer 2100 (Agilent, Agilent HS DNA Reagent, 5067–4627). The concentration and quality of

target enriched sequencing libraries were tested by Qubit (Invitrogen). Finally, the libraries were loaded on Illumina HiSeq 4000 according to the manufacturer's instrument.

'G3viz' is an R package to visualize location and frequency of mutations in *TP53* [21]. The R package 'ComplexHeatmap' was used to analyze the mutated genes in *TP53*-mut DLBCL [22].

RNA sequencing

Library construction

Total RNA was isolated using TRIzol RNA Isolation method (Invitrogen). Ribosomal RNA was eliminated by RNase H and the sequencing library was prepared by KAPA Stranded RNA-seq Kit with RiboErase (HMR) (KAPA Biosystems). Library was sequenced by Illumina HiSeq NGS platforms (Illumina), following concentration measurements and regular quality assessments.

Gene expression analysis

To generate sequence reads, base calling was performed with bcl2fastq v2.19.0.316 (Illumina) following quality control (QC) analysis of sequence reads to determine if the sequencing data is suitable for subsequent analysis [23]. R packages 'DESeq2' and 'limma' were used to analyze differential expression in patients and cell lines, respectively [24, 25]. We selected differentially expressed genes (DEGs) with *P*-values 0.05 and fold-changes >1.0 as significant and used them in our analysis. Gene Set Enrichment Analysis (GSEA) was performed to decipher the meaningful signaling pathways and biological processes in the enrichment analysis of differentially expressed genes [26]. Gene Ontology (GO) and Kyoto Encyclopedia of Genes and Genomes (KEGG) annotation was performed with the R package 'clusterProfiler' to further elucidate the biological role of DEGs [27]. The 'oncoPredict' R package was used to predict the half-maximal inhibitory concentration (IC50) values in patients in the different risk groups [28].

Determination of immune cell infiltration

To estimate the scores for immune cell types in the tumor microenvironment, single-sample gene set enrichment analysis (ssGSEA) was used. Based on gene expression levels in a single sample, enrichment scores are calculated, and these scores are then normalized [29]. Then, enrichment score of inflammatory cytokines and immune checkpoints (ICPs) was calculated using ssGSEA. Table S2 summarizes the genesets applied.

Statistical analysis

All statistical analyses were performed with SPSS statistics version 20.0, GraphPad Prism version 7.0 statistical software and R software (Version 4.1.3). Unpaired Students' *t*-tests were used for comparing normally

distributed variables. The correlation analysis was actualized by Spearman's correlation test. The Kaplan–Meier method and Log-Rank or Breslow tests were used for survival analysis. Cox proportional hazards regression models were used for univariate and multivariable analysis. The forest plot was utilized to visualize the results of univariate and multivariate Cox regression analyses. *P*<0.05 was considered statistically significant. Graphs were made with GraphPad Prism 7, the "ggplot2" and "ComplexHeatmap" R package.

Results

Mutation profile and prognostic impacts of *TP53* mutations in DLBCL

Among the 2637 DLBCL patients from the integrated cohort, 2267 patients (86.0%) were *TP53* wild-type (*TP53*-wt) while *TP53* mutations were found in 370 patients with a 14.0% mutation rate, including 305 with missense mutations, 32 with nonsense mutations, 26 with multiple mutations, 25 with frameshift mutations, 16 with splicing site mutations, 5 with intronic mutations, 3 with in frame mutations, 3 with loss of stop and 1 with start lost (Fig. 2A). The distribution of mutation events detected in the 370 patients were mainly located in the DNA binding domain (DBD) (*N*=333, 90.0%), containing 34 at Arg248, 20 at Gly245, 20 at Arg273, 18 at Arg175, 12 at Arg282, corresponding to the *TP53* hotspots in non-Hodgkin lymphoma described in previous studies [11, 30] (Fig. 2B). In the structural motif corresponding to the domain functional region, 36% of mutations have been located in the L2/L3, 35% in the NDBL/beta-sheets, and 21% in the L1/S/H2 (Fig. 2C). In the integrated cohort, *TP53* mutations were detected scattered throughout exon 2 to exon 11, with 35% in exon 7, 21% in exon 5, 19% in exon 8, 15% in exon 6, 5% in exon 4 and 5% in other exons (Fig. 2E). *TP53* mutations were predominated by C>T (*N*=125, 35%) and G>A (*N*=66, 18%) transitions, and the overall transition rate was 70% with the transition/transversion ratio of 2.3 (Fig. 2F).

M. Staudt and colleagues identified seven genetic subgroups and developed the LymphGen algorithm, which allows a precise genetic classification for DLBCL patients⁸. We acquired the LymphGen genetic subtype information from the supplement data of published articles, including Lacy S et al. cohort [15], Pedrosa L et al. cohort [19] and Chapuy B et al. cohort [1]. Furthermore, we used the LymphGen algorithm web tool (<https://lmpp.nih.gov/lymphgen/index.php>) to distinguish the genetic subtypes for Reddy A cohort and TCGA cohort patients. In this part of the analysis, Dubois S cohort was removed because of limited genes in the NGS panel. Most of the *TP53*-mut DLBCL patients in the integrated cohort can be classified into other subtype (58%) due to

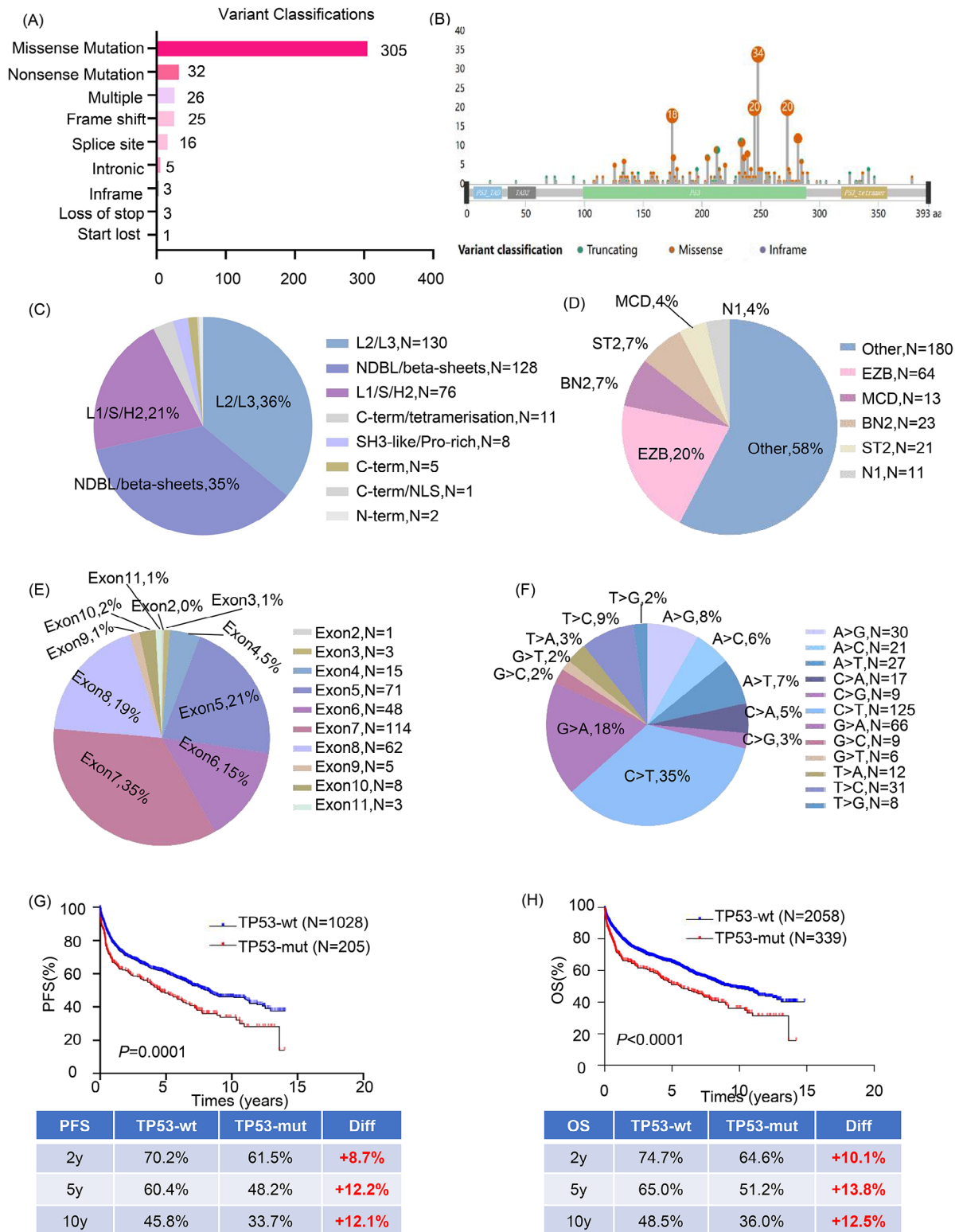


Fig. 2 TP53 mutations and prognostic impact in DLBCL. (A) The proportion of TP53 mutation types in TP53-mut DLBCL patients. (B) Lollipop plot illustrating specific localization of TP53 variants. (C) Donut graph demonstrating proportion of TP53 mutation according to Structural motif. (D) Donut graph demonstrating proportion of TP53 mutation according to LymphGen subtype (N1, ST2, BN2, MCD, EZB and Other). (E) Donut graph demonstrating proportion of TP53 mutation according to different base substitution. (F) Donut graph demonstrating proportion of TP53 mutation according to different base substitution. (G) PFS analysis based on TP53 mutational status in DLBCL patients. (H) OS analysis based on TP53 mutational status in DLBCL patients. PFS, progression free survival; OS, overall survival; TP53-wt, wild-type TP53; TP53-mut, mutated TP53; Diff, difference; DLBCL, diffuse large B-cell lymphoma

Table 1 Clinical characteristics of 2637 cases of DLBCL according to the *TP53* mutational status

Characteristics	Total	<i>TP53</i> -wt (N=2267)	<i>TP53</i> -mut (N=370)	P-value
Gender				0.196
Female	816	735	81	
Male	971	856	115	
Unknown	850	676	174	
Age				0.039
≤60y	919	806	113	
>60y	1652	1400	252	
Unknown	66	61	5	
Stage				0.717
I/II	684	609	75	
III/IV	1032	913	119	
Unknown	921	745	176	
No. of extranodal sites				0.599
Fewer than 2	938	844	94	
At least 2	279	248	31	
Unknown	1420	1175	245	
Serum LDH level				0.026
Normal	699	630	69	
Elevated	911	788	123	
Unknown	1027	849	178	
ECOG				0.712
0~1	1270	1126	144	
2~4	374	329	45	
Unknown	993	812	181	
Subtype				0.098
GCB	781	654	127	
ABC	702	605	97	
UNC	265	237	28	
Unknown	889	771	118	
IPI risk group				0.243
Low	514	453	61	
Intermediate	1130	969	161	
High	452	382	70	
Unknown	541	463	78	
aalPI risk group				0.088
Low	151	142	9	
Low-Intermediate	171	148	23	
High-Intermediate	175	150	25	
High	88	77	11	
Unknown	334	289	45	
LymphGen subtype				<0.001
Other	1387	1207	180	
BN2	172	149	23	
EZB	373	309	64	
MCD	172	159	13	
N1	25	14	11	
ST2	147	126	21	

missing the data of copy-number, followed by EZB (20%), MCD (4%), BN2 (7%), ST2 (7%) and N1(4%) (Fig. 2D).

The clinical parameters between the *TP53*-mut and *TP53*-wt groups in the integrated cohort are summarized in Table 1. Of note, there is a significantly higher frequency of elevated LDH levels ($P=0.026$) and older age ($P=0.039$) in *TP53*-mut patients. Compared with *TP53*-wt patients, the *TP53*-mut patients were associated with significantly worse survivals of 2-year, 5-year and 10-year PFS (61.5% vs. 70.2%, 48.2% vs. 60.4%, 33.7% vs. 45.8%, $P=0.0001$, Fig. 2G), which were similar to data in previous research [30]. In terms of OS, a significant P value was generated ($P<0.0001$, Fig. 2H).

However, after reviewing clinical course of patients with *TP53* mutation in our center's cohort, we found that actually not all the *TP53*-mut patients acquired poor clinical outcomes. The different outcomes of such typical *TP53*-mut patients have caught our attention. Furthermore, the differences of 2-year, 5-year and 10-year PFS and OS between *TP53*-mut and *TP53*-wt patients were all less than 15% (Fig. 2G and H). Therefore, more precise stratification is worth investigating for *TP53*-mut DLBCL patients.

Identify genetic risk factors for *TP53*-mut DLBCL patients

The above findings prompted us to further consider if we could construct a model to identify the truly high-risk *TP53*-mut DLBCL patients. First, we retrieved the *TP53* database (<https://TP53.isbcgc.org/> originally IARC database) for *TP53* mutation site information of the six cohorts in order to obtain additional information about *TP53* mutations and functions. Based on all the information contained in the *TP53* database, we conducted survival analysis, and Fig. 3 summarizes some important results. Compared with patients with missense mutations, patients with non-missense mutations have a significantly poorer survival ($P=0.0473$, Fig. 3A), and patients with multi-site mutations also have a significantly poorer survival ($P=0.0368$, Fig. 3D). While most mutations affecting P53 protein function result in loss of function, there are still 6.1% of notDNE_notLOF patients who have no effect on P53 protein function and have a good prognosis ($P=0.0363$, Fig. 3B). In terms of structure function, the result is similar, with a statistical trend ($P=0.0855$, Fig. 3C). Additionally, mutations at splicing sites ($P=0.1172$, Fig. 3F) and non-hotspot mutations ($P=0.1175$, Fig. 3G) had a poor prognosis, with a statistical trend. Using X-tile for the optimal cutoff, variants with VAF>36% were considered high burden, and high VAF was associated with worse prognosis ($P<0.0001$, Fig. 3H). The prognosis of these missense mutation patients is not differentiated according to whether the mutation occurs within the DNA-binding loops or not (Fig. 3E).

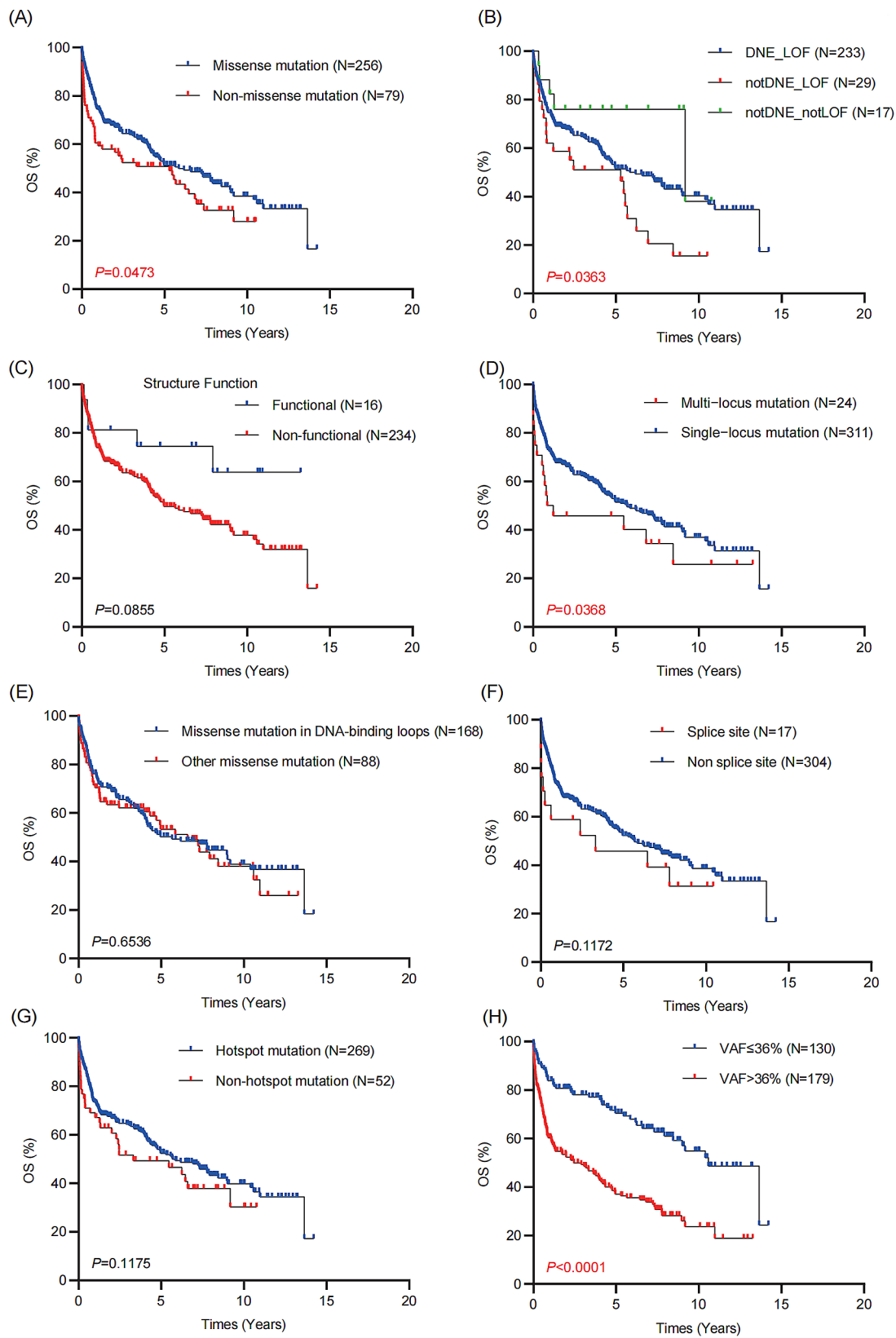


Fig. 3 The Kaplan-Meier curves of mutation-related characteristics for *TP53*-mut patients. **(A)** Mutation types ($P=0.0473$). **(B)** DNE_LOF class ($P=0.0363$). **(C)** Structure function class ($P=0.0855$). **(D)** Multi-local mutations ($P=0.0368$). **(E)** Missense mutation in DNA-binding loops ($P=0.6536$). **(F)** Splice site ($P=0.1172$). **(G)** Hotspot mutation ($P=0.1175$). **(H)** Variants >36% VAF are considered high burden by using X-tile to select the optimal cutoff value ($P<0.0001$). OS, overall survival; DNE, dominant negative effective; LOF, loss-of-function; VAF, variant allele frequency

Since missense mutations account for the vast majority of *TP53*-mut DLBCL patients (Fig. 2A and B) and most of non-missense mutations can affect the function of P53 protein which ultimately leads to worse survivals (Fig. 3A). Therefore, we attempted to further stratify missense mutation patients.

Construction of a prognosis signature for *TP53* missense mutation DLBCL patients based on integrative machine learning

The dataset was divided into a training set and an internal testing set at a 4:1 ratio. In the training set, we fitted 150 prediction models with a tenfold cross-validation framework and computed the C index across all training and testing sets, the top 50 out of 150 kinds of prediction models as illustrated in Fig. 4A. The calibration curves showed good agreement between the top 3 prediction models predictions and actual observations (Figure S1A and S1B). Next, we followed two models - the RSF and the Ridge+RSF, both of which demonstrated good predictive abilities in both training and testing cohort. However, Ridge+RSF is more concise, yet equally effective predictive model than RSF, which incorporates more

factors. As a result of comprehensive screening, we identified Ridge+RSF as a predictive model.

Through a tenfold cross-validation framework, we determined that 0.285266 was the optimal λ value in the Ridge analysis by minimizing the partial likelihood deviation (Fig. 4B and C). Figure 4D shows the importance ranking of each variable. Further, we performed COX multivariate regression analysis on these important variables and selected 4 independent prognostic variables to establish the *TP53* missense mutation risk model (Fig. 4E). The coefficients for each variable are shown in Fig. 4F. The C index demonstrates the stable and robust predictive ability of the *TP53* missense mutation risk model in both training and testing cohort (Figure S1C and S1D). The AUC of the model achieved 0.676 and 0.663 in training and testing cohort, respectively, indicating its predictive accuracy (Figure S1E and S1F). In order to divide patients with *TP53* missense mutations into low-risk and high-risk groups, we selected a risk score of -0.34484, which is close to 50%, as the cutoff value for dividing patients with *TP53* missense mutations. Details were shown in Fig. 4G. In the whole cohort and testing cohort, patients in the high-risk group

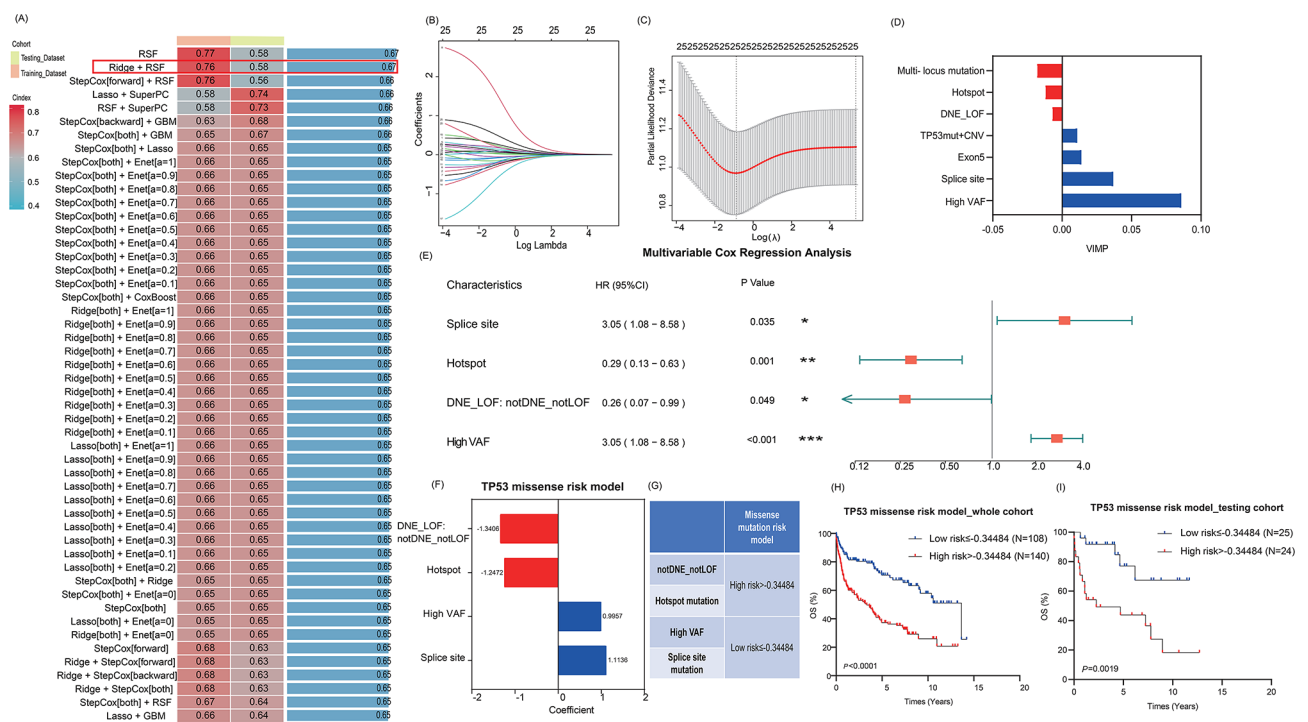


Fig. 4 A *TP53* missense mutation risk model is developed and validated via the machine learning and COX multivariate regression analysis-based integrative procedure. (A) Heatmap shows the top 50 out of 150 kinds of prediction models along with their C-indices across all training and testing datasets. (B,C) Visualization of Ridge regression in the training cohort. The optimal λ was obtained when the partial likelihood deviance reached the minimum value. (D) The RSF algorithm is then used to screen key factors and visualize the VIMP. (E) Four statistically significant factors are ultimately screened out using COX multivariate regression analysis. (F,G) Regression coefficients of 4 key factors obtained in COX multivariate regression to construct the *TP53* missense mutation risk model. (H, I) Kaplan–Meier curves of OS according to the *TP53* missense mutation risk model in the whole cohort ($P < 0.0001$) and testing cohort ($P = 0.0019$). * $P < 0.05$, ** $P < 0.01$, and *** $P < 0.001$. RSF, random survival forest; GBM, gradient boosting machine; DNE, dominant negative effective; LOF, loss-of-function; *TP53*-mut, mutated *TP53*; CNV, copy number variant; VAF, variant allele frequency; VIMP, variable importance; HR, Hazard Ratio; 95%CI, 95% Confidence Interval; OS, overall survival

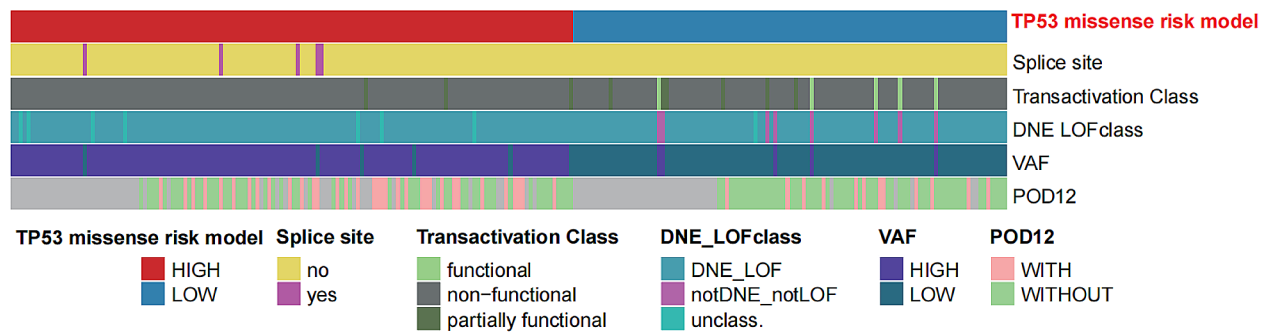
exhibited significantly worse OS than those in the low-risk group (Fig. 4H and I).

Differences in clinical characteristics between the two risk groups of TP53 missense mutation

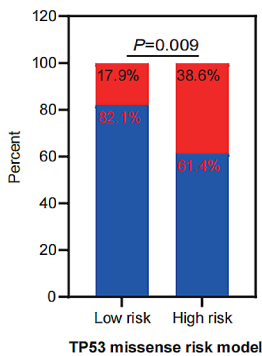
The clinical and mutation features were evaluated between the two risk groups of TP53 missense mutation in the whole cohort. We found that the splice site

mutation, transactivation class, DNE_LOF class and VAF were significantly correlated with the risk groups, but other clinical characteristics except POD12 did not show significant differences (Fig. 5A and S2). And we observed significant difference in the distribution of POD12 between the high- and low-risk groups ($P=0.009$, Fig. 5B). These findings suggested that high-risk TP53

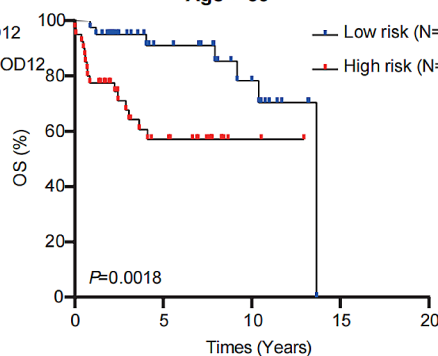
(A)



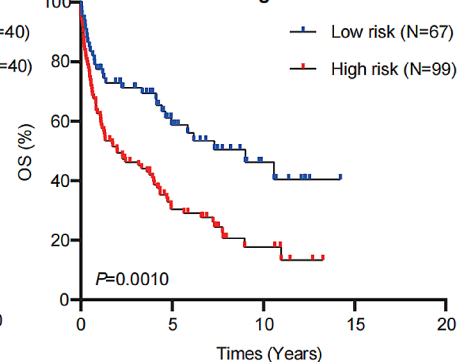
(B)



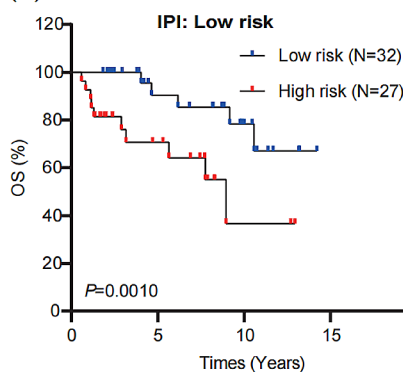
(C) Age ≤ 60



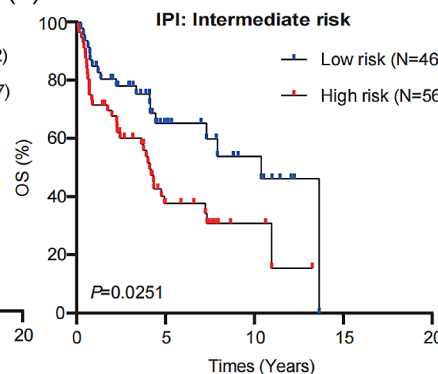
(D) Age > 60



(E) IPI: Low risk



(F) IPI: Intermediate risk



(G) IPI: High risk

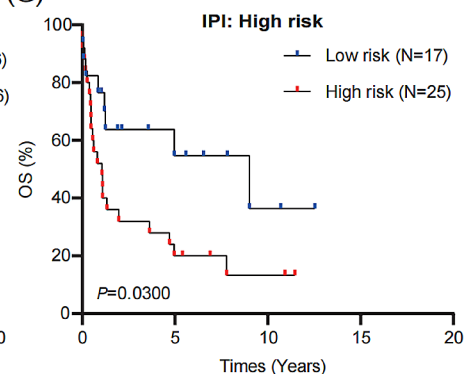


Fig. 5 Clinical characteristics and prognosis of DLBCL patients with TP53 missense mutations who are divided into high-risk and low-risk groups based on the TP53 missense mutation risk model. (A) Heatmap showing the comparison of the clinical and mutation characteristics of patients with DLBCL in TP53 missense mutation high risk and low risk. (B) The proportion of POD12 in TP53 missense mutation risk subgroups. (C–G) Kaplan–Meier curves showing stable performance of the TP53 missense mutation risk model in the subgroups of DLBCL patients, including age and IPI stratification. * $P < 0.05$, ** $P < 0.01$, and *** $P < 0.001$. DNE, dominant negative effective; LOF, loss-of-function; VAF, variant allele frequency; IPI, International Prognostic Index; POD12, progression of disease within 12 months; OS, overall survival

missense mutation patients are associated with early progression.

By performing Kaplan-Meier curve analysis, we also found that the risk model demonstrated a robust prognostic ability for *TP53* missense mutation DLBCL patients across subgroups stratified by various clinical characteristics, including age and IPI (Fig. 5C–5G).

Biological mechanisms underlying different prognosis of *TP53*-mut DLBCL patients

To elucidate the underlying biological mechanisms in *TP53*-mut DLBCL and subtypes, we performed genetic mutation landscape analysis by somatic mutation data and differential expression analysis by using RNA-seq in JSPH cohort. JSPH cohort's clinical parameters were summarized in Table S3. Among them, 24 patients with *TP53* missense mutations were stratified according to the above *TP53* missense mutation risk model, with 12 patients at low risk and 12 patients at high risk.

Based on the stratification of the *TP53* missense mutation risk model, the oncoplot indicated that *CCND3* mutants were significantly more prevalent in the high-risk group (Fig. 6A). 2498 DEGs including 2079 down-regulated and 419 upregulated genes were enriched in high-risk *TP53* missense mutation DLBCL (Fig. 6B). As expected, the immune-associated biological processes occupied a large proportion in the result of GO functional enrichment analysis (Fig. 6C). The KEGG enrichment analysis also revealed that *TP53* missense mutation high-risk patients had dysregulation of multiple immune, metabolic, adhesion, and carcinogenic pathways (Fig. 6D). As well, Figure S3A and S3B showed the differentially expressed and enrichment analyses between wild type and mutant *TP53*.

We estimated the relative abundances of infiltrating immune subpopulations by ssGSEA and found that CD8⁺ T cells, checkpoints, cytolytic activity, Th1 cells, and Th2 cells were exhausted in the *TP53*-mut group with a characteristic immune microenvironment (Figure S3C). Furthermore, we found that the high-risk *TP53* missense mutation DLBCL lacked multiple immune cells, including neutrophil, type 17 T helper cell, mast cell, type 2 T helper cell, type 1 T helper cell, effector memory CD4 T cell, CD56bright natural killer cell, immature dendritic cell, plasmacytoid dendritic cell, effector memory CD8 T cell, and central memory CD4 T cell (Fig. 6E). In order to examine the inflammatory cytokines, we used the Wilcoxon test to compare the cytokine expression levels among the various *TP53* missense mutation DLBCL risk groups. As a result, the expression levels of *IL1*, *IL-5*, *IL-7*, *IL-15*, and *MCP-1* were significantly down-regulated in missense mutation high-risk group (Figure S4A). ICPs reflect the immune status of the tumor microenvironment. The expression levels of 46 ICP-related modulators

were further analyzed, and we found that *BTLA*, *CD200*, *CD244*, *CD28*, *CD40LG*, *CTLA4*, *IDO1*, *IDO2*, *LAG3*, *LGALS9*, *PDCD1*, *TMIGD2*, *TNFRSF18*, *TNFRSF25*, *TNFRSF14*, and *TNFRSF15* were dramatically downregulated in high-risk group ($P < 0.05$, Figure S4B), resulting in unfavorable prognosis. Taken together, the *TP53* missense mutation risk model was related to the immune response.

The IC50 analysis using 'oncoPredict' predicted that patients in high-risk group were more sensitive to TW 37_1149, Shikonin_170, Motesanib_1029, and NU7441_1038 compared to the low-risk group and the non-missense mutation group (Figure S5A–S5D). Compared to the non-missense mutation group, the high-risk group had greater sensitivity to multiple kinase inhibitors (Dabrafenib_1373, Olaparib_1017, Veliparib_1018, Rucaparib_1175, Pilaralisib_372, Dactolisib_1057), antimetabolites (Pemetrexed_428, Cytarabine_1006), DNA damaging agents (Cisplatin_1005), P53 transcriptional activity activator (Tenovin-6_342), and Pevonedistat_1529 (Figure S5E–S5O). Additionally, AKT inhibitor VIII_228 was more suitable for patients in low-risk group (Figure S5P).

We employed GSEA to acquire the enrichment pathway of DLBCL cell lines grouped in several ways in the CCLE databases. The information about the 21 cell lines is presented in Table S4. In MCD subtype cell lines, the KEGG data shed light on the *TP53* mutation positively regulated cell cycle and DNA replication pathway, as did KEGG enrichment analysis in EZB subtype cell lines; moreover, the carbon metabolism reprogramming was more enriched in the ST2 subtype [8] (Figure S6A–S6F). By contrast, *TP53* mutation was predicted to be a positive regulator of the lysosome and oxidative phosphorylation pathway in other subtype of DLBCL cell lines (Figure S6G and S6H).

*TP53*PI for precise stratification for *TP53*-mut DLBCL patients

The Kaplan-Meier curve survival analysis was then performed for the stratified *TP53* missense mutation patients, non-missense mutation patients, and wild-type patients. No difference in survival was observed between patients with high-risk *TP53* missense mutation and those with non-missense mutation ($P = 0.9164$, Fig. 7A), while there was no difference between patients with low-risk missense mutation and wild-type patients ($P = 0.1311$, Fig. 7A). Therefore, in our more comprehensive study of *TP53* mutations, DLBCL patients with high-risk missense mutation were treated equally to those with non-missense mutation. Based on the univariate Cox regression result described in Figure S7, significant variables were further performed multivariate Cox regression analysis. As shown in Fig. 7B, two variables

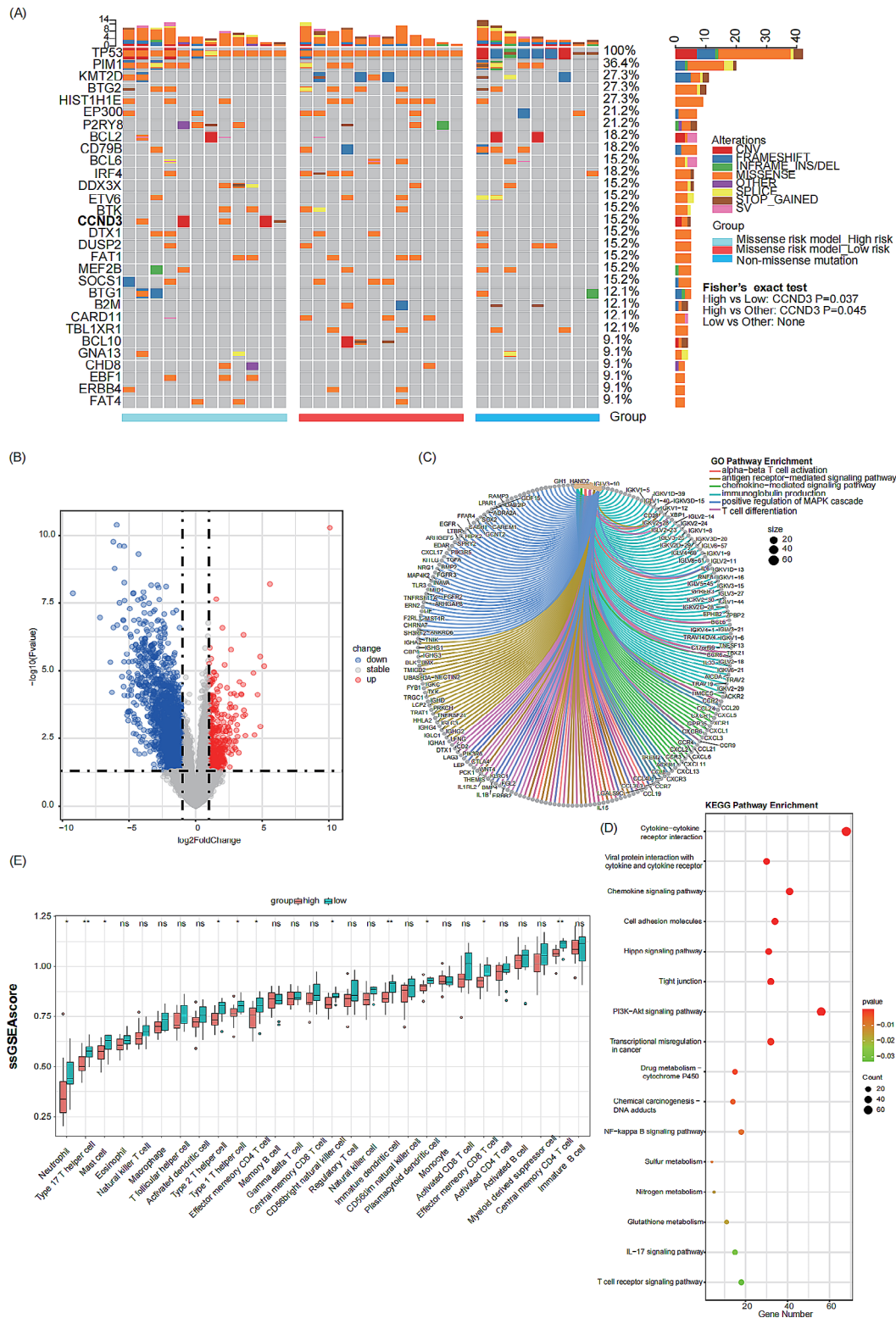


Fig. 6 Biological mechanisms underlying different prognosis of *TP53* missense mutation DLBCL patients. **(A)** Oncoplot illustrating the mutated genes in *TP53* missense mutation DLBCL patients. **(B)** Volcano plot showing upregulated and downregulated genes between high-risk and low-risk *TP53* missense mutation DLBCL. **(C)** Chord plot of GO analysis on immune-related pathway. **(D)** KEGG pathway enrichment plots of the DEGs between high-risk and low-risk *TP53* missense mutation DLBCL. **(E)** Boxplot of the abundances of infiltrating immune cell subpopulations between high-risk and low-risk *TP53* missense mutation DLBCL according to the ssGSEA algorithm. * $P < 0.05$, ** $P < 0.01$, and *** $P < 0.001$. GO, Gene ontology; KEGG, Kyoto Encyclopedia of Genes and Genomes

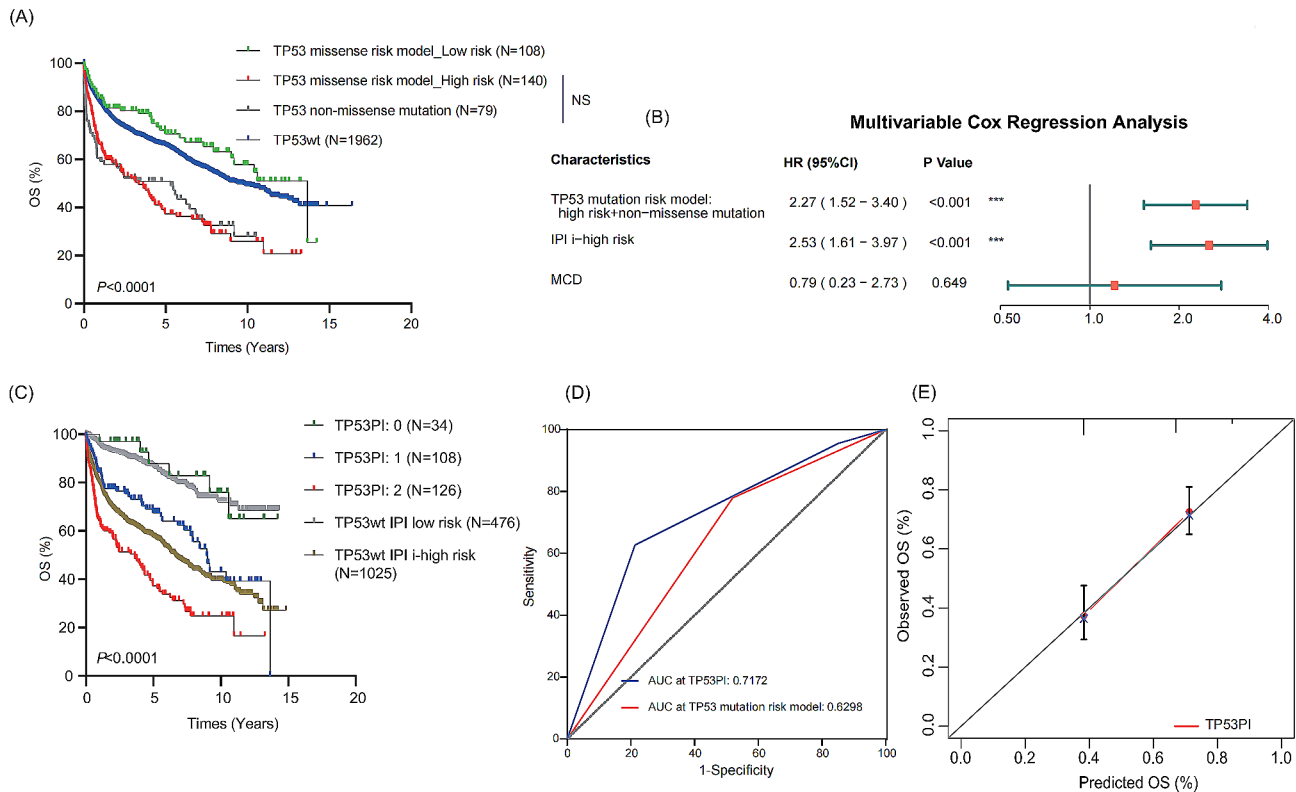


Fig. 7 The establishment of the TP53PI model. **(A)** Kaplan-Meier curves for *TP53* missense mutation risk model vs. *TP53* non-missense mutation vs. *TP53*-wt patients ($P < 0.0001$). **(B)** Forest plot shows a multivariate Cox analysis of OS for *TP53*-mut patients including clinical and biological characteristics. **(C)** Kaplan-Meier curves of *TP53*-mut DLBCL patients according to TP53PI model risk stratifications and those of *TP53*-wt DLBCL patients according to IPI risk stratifications. **(D)** ROC curves of TP53PI and *TP53* mutation risk model. **(E)** Calibration curve of the TP53PI model. * $P < 0.05$, ** $P < 0.01$, and *** $P < 0.001$. OS, overall survival; *TP53*-wt, wild-type *TP53*; HR, Hazard Ratio; 95%CI, 95% Confidence Interval; IPI, International Prognostic Index; TP53PI, *TP53* prognostic index; AUC, area under the curve; ROC, receiver operator characteristic

(*TP53* missense mutation high risk + non-missense mutation and IPI intermediate- or high-risk groups) retained independent prognostic significance, which constituted TP53PI model. As the coefficients of the two variables in the multivariate COX regression are similar, 0.8214 and 0.9268, respectively, we simplified the model and set the score of these two variables to 1. The specific risk grades in TP53PI model are described as follows: (1) low risk, score=0; (2) intermediate risk, score=1; and (3) high risk, score=2. The Kaplan-Meier curves for the TP53PI model were plotted ($P < 0.0001$, Fig. 7C). In addition, the survival of the TP53PI low-risk group is similar to that of the *TP53*-wt IPI low-risk group ($P = 0.6344$, Fig. 7C), while the survival of the TP53PI intermediate risk group and the *TP53*-wt IPI intermediate-high risk group did not differ ($P = 0.0672$, Fig. 7C). ROC analysis displayed that the risk stratification of TP53PI model had better discrimination to *TP53* missense mutation risk model + non-missense mutation for OS (AUC: 0.7172 vs. 0.6298, Fig. 7D). Moreover, the calibration plots demonstrated good concordance between predicted and observed probabilities (Fig. 7E).

Discussion

Up to this point, the prognostic significance of *TP53* mutation in DLBCL patients has been debated in several previous studies [31]. Hong Y et al. recently analyzed DLBCL patients with *TP53* mutation for preliminary stratification [11]. A *TP53* mutation rate of 16% was observed in their analysis, and the profile of *TP53* mutations was predictive of poor OS and PFS, despite the close survival curves between the two groups. According to subgroup analysis, they found that *TP53* mutation differed in prognostic significance among different subgroups.

In view of the diversity and heterogeneity of *TP53* gene mutations and functional variations, the impact of each mutation/variation on a specific patient's prognosis should be evaluated individually based on the type, site, and affected target genes. According to the traditional view of determining a "good prognosis" or a "poor prognosis" based only on the status of *TP53* gene, which can be either wild type or mutant, is inaccurate. The impact of *TP53* mutations on prognosis varies greatly among different molecular subtypes: in *MYD88* and *BCL-2* subtypes, *TP53* mutations indicate poor prognosis; in

NOTCH2 or *SOCS1/SGK1* subtypes, *TP53* mutations have no significant impact on prognosis; and in the *TET2/SGK1* subtype, *TP53* mutations are rare [15].

We examined the clinical features and *TP53* mutation data of 2637 reported cases in order to identify the characteristics and prognostic significance of *TP53* mutation in DLBCL patients in the present study. We revealed a *TP53* mutation prevalence of 14.0% in DLBCL patients, which is lower than those of previous reports in DLBCL (20–25%) [32]. The majority of *TP53* mutations was missense mutation, and most mutations occurred in the DBD, with hot spots at codons 248, 245, 273, 175 and 282, suggesting these motifs were essential for *TP53* tumor suppression.

This finding of our study and clinical practice suggested that not all patients with *TP53* mutations had a fatal outcome. Therefore, our research aims to construct an innovative model to predict prognosis and accurately distinguish the risks of *TP53*-mut DLBCL patients. It will facilitate the prediction and treatment of *TP53*-mut DLBCL. Furthermore, we attempt to investigate the molecular mechanisms behind these characteristics using multi-omics methods. In this way, the correlation between the mutation of *TP53* and prognosis or response to treatment can be understood on a molecular level.

We successfully fitted a model with high predictive accuracy and applicability, which reduces the dimensionality of variables and simplifies the model. The model includes four indicators: splice site mutation, high VAF (VAF > 36%), hotspot mutations, and notDNE_notLOF. Previous studies have reported that some hotspot mutations of *TP53* (e.g. c.659 A > G, p.Y220C, c.733G > A, and p.G245S) have immunogenicity in ovarian cancer, which may indicate that they play a role in the immune response [33]. However, this does not mean that these mutations are protective factors. Instead, they may be related to the activation of the immune system, thereby affecting prognosis. In addition, non-disruptive mutations in the *TP53* DNA-binding domain are also considered an independent favorable prognostic factor in esophageal squamous cell carcinoma [34]. The notDNE_notLOF indicates that the *TP53* mutation has not affected the normal function of the P53 protein.

We further found that there is no difference in survival between the high-risk group of *TP53* missense mutation and non-missense mutation patients. To stratify the entire population of *TP53* mutation, we ultimately construct the TP53PI model.

NGS has been widely applied in clinical samples, leading to several reclassification schemes being proposed in previous studies [1, 35], including the LymphGen arithmetic which is most commonly used [8]. *TP53* mutations and deletions were set to A53 subtype. However, in A53 type, there are a great many features associated with

chromosomal arms variations, which are challenging to detect with existing NGS methods. Applying the LymphGen classifier, less than half of *TP53*-mut DLBCLs were classified as one of the established molecular DLBCL subtypes highlighting the unique biology of this entity (Fig. 2D). Due to different mutation status of the LymphGen subtypes and distinct microenvironmental compositions, they responded differently to therapy targeting oncogenic signal pathways and immunotherapy. A53 displayed relatively low levels of all immune signatures. In addition, *B2M* is deleted or mutationally inactivated, allowing A53 patients to escape immune surveillance [36, 37].

Furthermore, we investigated the potential mechanisms of *TP53* missense mutation heterogeneity at both the genomic and transcriptomic levels. In the high-risk group, immune, metabolic, adhesion, and PI3K-AKT signaling pathways are dysfunctional. Inspired by these findings in previous studies, we focused on immune-related pathways and examined the immune-infiltrating microenvironment of the *TP53* missense mutation high-risk DLBCLs. Our results show that the high-risk group has an absolute immune-suppressive microenvironment, with a reduced number of various immune cells, which are anti-tumor immune cells. The analysis of immune checkpoints also shows a generally downregulated state in the high-risk group, with a reduction in the number of immune cells or impaired function, which may not be sufficient to promote an effective immune response and may further adversely affect the effects of immunotherapy.

As a result of oncoPredict's drug sensitivity prediction results, patients in *TP53* missense mutations high-risk group are likely to be more sensitive to kinase inhibitors and *MCL1* inhibitors, than other *TP53*-mut DLBCL patients. Among them, *MCL1* inhibitors (TW37) may be effective for *TP53* missense mutations high-risk DLBCL patients, especially when used in combination with other drugs. The *MCL1* protein belongs to the *BCL-2* family of anti-apoptotic proteins. *BCL-2* inhibitor venetoclax/ABT-199 has been approved for the treatment of chronic lymphocytic leukemia (CLL) and acute myeloid leukemia (AML) [38, 39]. In spite of the fact that venetoclax initially responds well in many patients, clinical data indicate that most patients will relapse, and the latest analysis indicates that CLL or AML with *TP53* mutation have a worse prognosis after venetoclax treatment than those with *TP53* wild type [40, 41]. PI3K inhibitors can reduce the phosphorylation of AKT and mTOR by blocking the activity of PI3K, thereby inhibiting the proliferation, survival, and metabolism of tumor cells. PI3K/AKT/mTOR signaling pathways are significantly disturbed in the high-risk group of patients with *TP53* missense mutations. PI3K inhibitors can reduce the energy supply and protein synthesis of tumor cells by blocking this pathway, thereby

inhibiting tumor growth. Tenovin-6 is a small molecule compound, which is a P53 activator, capable of stabilizing and activating P53 by binding to the MDM2 inhibitor of the P53 protein, thereby activating the P53-mediated signaling pathway [42]. It appears that this drug is more suitable for the treatment of patients in high-risk groups. Due to the complexity of the P53 regulatory network, it is difficult to overcome the adverse effects of *TP53* mutations by blocking a single pathway, so it is necessary to further seek appropriate combination schemes to improve the therapeutic effect.

In the MCD and EZB subtype, the presence of a *TP53* mutation could potentially lead to an upregulation or enhanced activity of genes involved in these pathways which are crucial for cell division and DNA synthesis. In the ST2 subtype, the KEGG data highlight a different pattern, which suggests that *TP53* mutations in this subtype might be associated with alterations in metabolic processes, potentially affecting how cells utilize and metabolize carbon sources for energy and biosynthesis. In contrast to the MCD and EZB subtypes, *TP53* mutations in other subtypes of DLBCL cell lines are predicted to be positive regulators of the lysosome and oxidative phosphorylation pathways. Oxidative phosphorylation is a process in cellular respiration that produces ATP. Enhanced oxidative phosphorylation could suggest a higher energy demand or an adaptation to metabolic stress. In summary, these results indicate that *TP53* mutations have different effects on cellular pathways in different DLBCL subtypes.

It is important to note that this study has some limitations. Data from the public database is partially missing, and further external data verification is necessary. Particularly, due to the lack of loss of the non-mutated allele in some cohorts and the different assessment criteria of various detection methods, we did not proceed with further analysis in this issue. In order to truly explain the particularity of the immune microenvironment, it is necessary to analyze the immune microenvironment by means more closed to the real state, such as single-cell RNA sequencing.

In conclusion, we developed a TP53PI model for precise risk stratification for *TP53*-mut DLBCL patients and the potential underlying mechanisms of different prognosis might be explained by the unique immune microenvironments.

Supplementary Information

The online version contains supplementary material available at <https://doi.org/10.1186/s12964-024-01765-w>.

Supplementary Material 1
Supplementary Material 2
Supplementary Material 3

Supplementary Material 4
Supplementary Material 5
Supplementary Material 6
Supplementary Material 7
Supplementary Material 8
Supplementary Material 9
Supplementary Material 10
Supplementary Material 11

Acknowledgements

Not applicable.

Author contributions

Kai-Xin Du, Yi-Fan Wu, Wei Hua and Jin-Hua Liang integrated and analyzed the data. Jin-Hua Liang and Kai-Xin Du provided technological assistance. Kai-Xin Du and Jun-Heng Liang performed bioinformatic analysis. Yi-Fan Wu, Wei Hua, Zi-Wen Duan, Hua Yin, Yue Li, Jia-Zhu Wu, Hao-Rui Shen, Rui Gao and Li Wang collected the clinical data for patients. Kai-Xin Du, Jin-Hua Liang, Wei Xu and Yi-Fan Wu prepared the manuscript. Wei Xu and Jin-Hua Liang supervised the study.

Funding

This research was funded by the National Natural Science Foundation of China (grant number 82200887 and 82370194), Jiangsu Science and Technology Department (grant number BK20220716 and BE2023780), China Postdoctoral Science Foundation (grant number 2022M711404 and 2023M741463), and Jiangsu Province Hospital (the First Affiliated Hospital with Nanjing Medical University) Clinical Capacity Enhancement Project (JSPH-MC-2022-13 and JSPH-MC-2022-21).

Data availability

The datasets used and analyzed during the current study are included in the manuscript and the supplementary materials.

Declarations

Ethics approval and consent to participate

This study was carried out according to the principles established by the Declaration of Helsinki and approved by the Ethical Committee of the Nanjing Medical University. All participants were provided with an informed consent that they signed prior to the experiments.

Consent for publication

Not applicable.

Competing interests

The authors declare no competing interests.

Received: 6 January 2024 / Accepted: 23 July 2024

Published online: 15 August 2024

References

1. Chapuy B, Stewart C, Dunford AJ, et al. Molecular subtypes of diffuse large B cell lymphoma are associated with distinct pathogenic mechanisms and outcomes. *Nat Med* May. 2018;24(5):679–90. <https://doi.org/10.1038/s41591-018-0016-8>.
2. Alizadeh AA, Eisen MB, Davis RE, et al. Distinct types of diffuse large B-cell lymphoma identified by gene expression profiling. *Nat* Feb. 2000;3(6769):503–11. <https://doi.org/10.1038/35000501>.
3. Thieblemont C, Briere J, Mounier N, et al. The germinal center/activated B-cell subclassification has a prognostic impact for response to salvage therapy in relapsed/refractory diffuse large B-cell lymphoma: a bio-CORAL study. *J Clin*

- Oncology: Official J Am Soc Clin Oncol Nov. 2011;1(31):4079–87. <https://doi.org/10.1200/jco.2011.35.4423>.
4. Gutiérrez-García G, Cardesa-Salzmann T, Climent F, et al. Gene-expression profiling and not immunophenotypic algorithms predicts prognosis in patients with diffuse large B-cell lymphoma treated with immunochemo-therapy. *Blood* May. 2011;5(18):4836–43. <https://doi.org/10.1182/blood-2010-12-322362>.
 5. Molina TJ, Canioni D, Copie-Bergman C et al. Young patients with non-germi-nal center B-cell-like diffuse large B-cell lymphoma benefit from intensified chemotherapy with ACVBP plus rituximab compared with CHOP plus ritux-imab: analysis of data from the Groupe d'Etudes des Lymphomes de l'Adulte/ lymphoma study association phase III trial LNH 03-2B. *Journal of clinical oncology: official journal of the American Society of Clinical Oncology*. Dec 10. 2014;32(35):3996–4003. <https://doi.org/10.1200/jco.2013.54.9493>
 6. Ott G, Ziepert M, Klapper W, et al. Immunoblastic morphology but not the immunohistochemical GCB/nonGCB classifier predicts outcome in diffuse large B-cell lymphoma in the RICOVER-60 trial of the DSHNHL. *Blood* Dec 2. 2010;116(23):4916–25. <https://doi.org/10.1182/blood-2010-03-276766>.
 7. Moskowitz CH, Zelenetz AD, Kewalramani T, et al. Cell of origin, germinal center versus nongerminal center, determined by immunohistochemistry on tissue microarray, does not correlate with outcome in patients with relapsed and refractory DLBCL. *Blood* Nov. 2005;15(10):3383–5. <https://doi.org/10.1182/blood-2005-04-1603>.
 8. Wright GW, Huang DW, Phelan JD, et al. A probabilistic classification Tool for genetic subtypes of diffuse large B cell lymphoma with therapeutic implica-tions. *Cancer cell* Apr. 2020;13(4):551–e56814. <https://doi.org/10.1016/j.ccell.2020.03.015>.
 9. Zenz T, Vollmer D, Trbusek M, et al. TP53 mutation profile in chronic lympho-cytic leukemia: evidence for a disease specific profile from a compre-hensive analysis of 268 mutations. *Leuk* Dec. 2010;24(12):2072–9. <https://doi.org/10.1038/leu.2010.208>.
 10. Flynt E, Bisht K, Sridharan V, Ortiz M, Towfic F, Thakurta A, Prognosis. Biol-ogy, and targeting of TP53 dysregulation in multiple myeloma. *Cells* Jan. 2020;24(2). <https://doi.org/10.3390/cells9020287>.
 11. Hong Y, Ren T, Wang X, et al. APR-246 triggers ferritinophagy and ferroptosis of diffuse large B-cell lymphoma cells with distinct TP53 mutations. *Leuk Sep*. 2022;36(9):2269–80. <https://doi.org/10.1038/s41375-022-01634-w>.
 12. Marks JA, Wang X, Fenu EM, Bagg A, Lai C. TP53 in AML and MDS: the new (old) kid on the block. *Blood Reviews* Feb. 2023;14:101055. <https://doi.org/10.1016/j.blre.2023.101055>.
 13. Canale M, Andrikou K, Priano I, et al. The role of TP53 mutations in EGFR-Mutated non-small-cell Lung Cancer: clinical significance and implications for Therapy. *Cancers* Feb. 2022;23(5). <https://doi.org/10.3390/cancers14051143>.
 14. Xu-Monette ZY, Wu L, Visco C, et al. Mutational profile and prognostic significance of TP53 in diffuse large B-cell lymphoma patients treated with R-CHOP: report from an International DLBCL Rituximab-CHOP Consortium Program Study. *Blood* Nov. 2012;8(19):3986–96. <https://doi.org/10.1182/blood-2012-05-433334>.
 15. Lacy SE, Barrans SL, Beer PA, et al. Targeted sequencing in DLBCL, molecu-lar subtypes, and outcomes: a Haematological Malignancy Research Network report. *Blood* May. 2020;14(20):1759–71. <https://doi.org/10.1182/blood.2019003535>.
 16. Sha C, Barrans S, Cucco F, et al. Molecular High-Grade B-Cell Lymphoma: defining a poor-risk group that requires different approaches to Therapy. *Journal of clinical oncology: official journal of the American Society of Clinical Oncology*. Jan. 2019;20(3):202–12. <https://doi.org/10.1200/jco.18.01314>.
 17. Reddy A, Zhang J, Davis NS, et al. Genetic and functional drivers of dif-fuse large B cell lymphoma. *Cell* Oct. 2017;5(2):481–e49415. <https://doi.org/10.1016/j.cell.2017.09.027>.
 18. Dubois S, Vially PJ, Bohers E, et al. Biological and Clinical Relevance of Associated genomic alterations in MYD88 L265P and non-L265P-Mutated diffuse large B-Cell lymphoma: analysis of 361 cases. *Clinical cancer research: an official journal of the American Association for Cancer Research*. May. 2017;1(9):2232–44. <https://doi.org/10.1158/1078-0432.Ccr-16-1922>.
 19. Pedrosa L, Fernández-Miranda I, Pérez-Callejo D, et al. Proposal and validation of a method to classify genetic subtypes of diffuse large B cell lymphoma. *Sci Rep* Jan. 2021;21(1):1886. <https://doi.org/10.1038/s41598-020-80376-0>.
 20. Chang MT, Bhattarai TS, Schram AM, et al. Accelerating Discovery of func-tional mutant alleles in Cancer. *Cancer Discovery* Feb. 2018;8(2):174–83. <https://doi.org/10.1158/2159-8290.Cd-17-0321>.
 21. Guo X, Zhang B, Zeng W, Zhao S, Ge D. G3viz: an R package to interactively visualize genetic mutation data using a lollipop-diagram. *Bioinf* (Oxford Eng-land) Feb. 2020;1(3):928–9. <https://doi.org/10.1093/bioinformatics/btz631>.
 22. Mayakonda A, Lin DC, Assenov Y, Plass C, Koeffler HP. Maftools: efficient and comprehensive analysis of somatic variants in cancer. *Genome Res* Nov. 2018;28(11):1747–56. <https://doi.org/10.1101/gr.239244.118>.
 23. Bolger AM, Lohse M, Usadel B. Trimmomatic: a flexible trimmer for Illumina sequence data. *Bioinformatics* (Oxford, England). Aug 1. 2014;30(15):2114–20. <https://doi.org/10.1093/bioinformatics/btu170>
 24. Love MI, Huber W, Anders S. Moderated estimation of Fold change and dispersion for RNA-seq data with DESeq2. *Genome Biol*. 2014;15(12):550. <https://doi.org/10.1186/s13059-014-0550-8>.
 25. Ritchie ME, Phipson B, Wu D, et al. Limma powers differential expression analyses for RNA-sequencing and microarray studies. *Nucleic acids research*. Apr. 2015;20(7):e47. <https://doi.org/10.1093/nar/gkv007>.
 26. Subramanian A, Tamayo P, Mootha VK, et al. Gene set enrichment analysis: a knowledge-based approach for interpreting genome-wide expression pro-files. *Proc Natl Acad Sci United States Am Oct*. 2005;25(43):15545–50. <https://doi.org/10.1073/pnas.0506580102>.
 27. Yu G, Wang LG, Han Y, He QY. clusterProfiler: an R package for compar-ing biological themes among gene clusters. *OmicS: J Integr Biology* May. 2012;16(5):284–7. <https://doi.org/10.1089/omi.2011.10118>.
 28. Maeser D, Gruener RF, Huang RS. oncoPredict: an R package for predicting in vivo or cancer patient drug response and biomarkers from cell line screening data. *Briefings Bioinf* Nov. 2021;5(6). <https://doi.org/10.1093/bib/bbab260>.
 29. Bindea G, Mlecnik B, Tosolini M, et al. Spatiotemporal dynamics of intra-tumoral immune cells reveal the immune landscape in human cancer. *Immun* Oct. 2013;17(4):782–95. <https://doi.org/10.1016/j.immuni.2013.10.003>.
 30. Young KH, Leroy K, Møller MB, et al. Structural profiles of TP53 gene mutations predict clinical outcome in diffuse large B-cell lymphoma: an international collaborative study. *Blood* Oct. 2008;15(8):3088–98. <https://doi.org/10.1182/blood-2008-01-129783>.
 31. Kastenhuber ER, Lowe SW. Putting p53 in Context. *Cell* Sep. 2017;7(6):1062–78. <https://doi.org/10.1016/j.cell.2017.08.028>.
 32. Peller S, Rotter V. TP53 in hematological cancer: low incidence of mutations with significant clinical relevance. *Hum Mutat* Mar. 2003;21(3):277–84. <https://doi.org/10.1002/humu.10190>.
 33. Deniger DC, Pasetto A, Robbins PF, et al. T-cell responses to TP53 hotspot mutations and unique neoantigens expressed by human ovarian cancers. *Clinical cancer research: an official journal of the American Association for Cancer Research*. Nov. 2018;15(22):5562–73. <https://doi.org/10.1158/1078-0432.Ccr-18-0573>.
 34. Huang M, Jin J, Zhang F, et al. Non-disruptive mutation in TP53 DNA-binding domain is a beneficial factor of esophageal squamous cell carcinoma. *Annals Translational Med* Mar. 2020;8(6):316. <https://doi.org/10.21037/atm.2020.02.142>.
 35. Schmitz R, Wright GW, Huang DW et al. Genetics and Pathogenesis of Diffuse Large B-Cell Lymphoma. *The New England journal of medicine*. Apr 12. 2018;378(15):1396–1407. <https://doi.org/10.1056/NEJMoa1801445>
 36. Challa-Malladi M, Lieu YK, Califano O, et al. Combined genetic inactivation of β 2-Microglobulin and CD58 reveals frequent escape from immune recogni-tion in diffuse large B cell lymphoma. *Cancer cell* Dec. 2011;13(6):728–40. <https://doi.org/10.1016/j.ccr.2011.11.006>.
 37. Godfrey J, Tumuluru S, Bao R, et al. PD-L1 gene alterations identify a subset of diffuse large B-cell lymphoma harboring a T-cell-inflamed phenotype. *Blood* May. 2019;23(21):2279–90. <https://doi.org/10.1182/blood-2018-10-879015>.
 38. Cang S, Iragavarapu C, Savooji J, Song Y, Liu D. ABT-199 (venetoclax) and BCL-2 inhibitors in clinical development. *J Hematol Oncol* Nov. 2015;20(8):129. <https://doi.org/10.1186/s13045-015-0224-3>.
 39. Nwosu GO, Ross DM, Powell JA, Pitson SM. Venetoclax therapy and emerging resistance mechanisms in acute myeloid leukaemia. *Cell Death Disease* Jun. 2024;12(6):413. <https://doi.org/10.1038/s41419-024-06810-7>.
 40. Stefanik P, Onyszczuk J, Szymczyk A, Podhorecka M. Therapeutic options for patients with TP53 deficient chronic lymphocytic leukemia: Narrative Review. *Cancer Manage Res*. 2021;13:1459–76. <https://doi.org/10.2147/cmar.S283903>.
 41. Santini V, Stahl M, Sallman DA. Jun. TP53 Mutations in Acute Leukemias and Myelodysplastic Syndromes: Insights and Treatment Updates. *American Society of Clinical Oncology educational book American Society of Clinical Oncology Annual Meeting*. 2024;44(3):e432650. https://doi.org/10.1200/edbk_432650

42. Lain S, Hollick JJ, Campbell J, et al. Discovery, in vivo activity, and mechanism of action of a small-molecule p53 activator. *Cancer cell* May. 2008;13(5):454–63. <https://doi.org/10.1016/j.ccr.2008.03.004>.

Publisher's Note

Springer Nature remains neutral with regard to jurisdictional claims in published maps and institutional affiliations.